The Effects of Interfacial Layers on the Open Circuit Voltage of Polymer:Fullerene Bulk Heterojunction Devices Studied by Charge Extraction Techniques

Chaiyuth Sae-kung,[‡,†] Brendan F. Wright[‡,¥], Tracey M. Clarke,[‡,§] Gordon G. Wallace[‡] and Attila J. Mozer[*,‡]

[‡] Intelligent Polymer Research Institute (IPRI), ARC Centre of Excellence for Electromaterials Science, AIIM, University of Wollongong, North Wollongong, NSW 2500, Australia.

[†]National Metal and Materials Technology Center, 114 Thailand Science Park, Paholyothin Rd., Klong 1, Klong Luang, Pathumthani 12120, Thailand.

[¥] School of Photovoltaic and Renewable Energy Engineering, University of New South Wales, Anzac Parade, 2052 Sydney, Australia

[§]Department of Chemistry, University College London, United Kingdom

ABSTRACT

Interfacial layers are frequently used in organic solar cells performing various functions, including blocking surface recombination, improving selectivity of charge carrier extraction, modification of the work function of the contact materials and enhancing light absorption within the photoactive layer through an optical cavity effect. The aim of this work is to investigate the origin of performance enhancement of bulk heterojunction solar cells using various electron and hole interfacial layers with a particular focus on the improvement to the open circuit voltage (V_{oc}). Solar cells using poly[N - 9′-hepta-decanyl-2,7-carbazole-alt-5,5-(4′,7′-di-2-thienyl-2′,1′,3′-benzothiadiazole)](PCDTBT) :)]:[6,6]-phenyl C70-butyric acid methyl ester (PC[70]BM) (1:4) active layers were prepared with a combination of polymeric, metal oxide and polyelectrolyte electron and or hole interfacial layers. Four device structures with i) no interfacial layers (reference); ii) only hole; iii) only electron; iv) both electron and hole interfacial layers were fabricated and compared using current-voltage, transient photovoltage and charge extraction measurements. The voltage gains (ΔV_{oc}) at matched charge density due to work function modification (ΔV_{oc}^{h} or ΔV_{oc}^{e}) is distinguished from the increase in V_{oc} due to increased charge carrier density due to longer charge carrier lifetime. At the hole contact, ΔV_{oc}^{h} was 0.21 V by using a PEDOT-PSS hole interfacial layer, while ΔV_{oc}^{e} was 0.29 V on the electron contact using a PEI-TiO$_x$ interfacial layer compared to reference devices. The electron lifetime also improved by orders of magnitude with the use of either electron or hole contact layers, contributing to a further 0.35 - 0.38 V increase in the open circuit voltage ((ΔV_{oc}^{rec}) due to increased charge density. The increased charge carrier lifetime is proposed to originate from the larger spatial separation of the electrons and holes in the device due to the increased internal field. Using both an electron and a hole interfacial layer didn't significantly increase the charge carrier lifetime compared to single

interfacial layer devices, therefore the V_{oc} didn't increase significantly. The findings presented clarify the role of interfacial layers in organic solar cells, and provides new insights into using time resolved charge extraction techniques to understand the influence of interfacial layers on the open circuit voltage.

INTRODUCTION

High performance organic solar cells would typically have one or two interfacial layers between the active layer and the electrical contacts.[1-3] Interfacial layers have been suggested to modify the work function of the electrodes, to improve the selectivity of electron and hole extraction,[2] to prevent surface recombination,[2, 4] to tune the optical electromagnetic field in the device through an optical cavity effect[5-6] and to enhance charge injection.[7] Maximizing these benefits and meeting some other practical requirements, such as processability of the photovoltaic layers,[8] stability of the electrodes[9-10] and cost,[8] constitute a significant effort of organic solar cell research and development. New active layer materials often require new contacts to be developed to reach their maximum performance. For example, low band gap polymers[11-14] with deep lying highest occupied molecular orbital (HOMO) levels require hole contact layers with higher work function.[15] New fullerene[16] and non-fullerene acceptors[17] with higher lying lowest unoccupied molecular orbitals (LUMO) require electron contacts with low work function.[18] Multi-junction tandem devices[19] and inverted structure solar cells[20] introduce further complexity in matching energy levels of the active layers and the electrodes.

Commonly used hole interfacial layers in organic solar cells include PEDOT-PSS (poly(3,4-ethylenedioxythiophene): poly(styrenesulfonate)),[7, 21] molydenum oxide(MoO_x),[22-29] nickel oxide (NiO),[30] vanadium oxide (V_2O_5),[21-22, 31] and tungsten trioxide (WO_3).[32] Commonly used electron interfacial layers include titanium oxide (TiO_x),[33-35] zinc oxide ZnO,[6, 20] cesium carbonate (Cs_2CO_3)[15] and lithium fluoride (LiF).[29] Polyelectrolytes, such as polyethoxylate imine (PEI) and polyethylenimine ethoxylated PEIE are an interesting class of materials as they can be used both as electron and hole interfacial layers.[36-37] Their function is proposed to originate from the interaction of the neutral amine groups with the surface of the contact material. For example, the

work function of ITO was lowered by almost 1 eV, which was attributed to the molecular dipoles of the ethylamine dipole as well as an interfacial dipole formed by physisorption of PEIE on the contact surface. [20, 34, 38]

Distinguishing the various effects of interfacial layers is often challenging experimentally. One of the key questions is to what extent interfacial layers increase the V_{oc} of the devices due to better work function alignment between the active materials and the contacts, as opposed to increased V_{oc} due reduced recombination. The effect of work function change has typically been inferred from the suppression of the dark current in reverse bias.[39] Steady state current-voltage measurements performed in the dark are also used to determine the diode ideality factors, which indicate the nature of recombination (surface, bulk or trap limited). Ideality factors derived from the light intensity dependence of the V_{oc} have been shown to yield a better analysis of recombination as it is not influenced by the devices' series resistance.[40] However, finite shunt resistance can still influence the measured ideality factors. Measurements of the ideality factors as a function of voltage was suggested to be preferred instead of an averaged value obtained from the V_{oc} versus light intensity curve. Reinhardt et al used a combination of current – voltage curves, electroluminescence (EL) measurements and numerical modelling to determine the selectivity of the contacts of bulk heterojunction solar cells. Enhanced rates of surface recombination yielded lower EL intensity, suggesting that surface recombination is a non-radiative process.[41] Wheeler et al. [42] has employed transient photovoltage and charge extraction measurements combined with simulations to analyze the increased V_{oc} of bulk heterojunction solar cells due to increased work function of the NiO hole contact. A large (407 mV) shift in the charge density versus V_{oc} plots were attributed to the increased splitting of the Fermi level at the contacts at the plasma treated NiO electrode. The V_{oc} increase due to longer charge carrier

lifetime was calculated (60 mV) at an intermediate charge density, suggesting that the main reason for the loss of V_{oc} is the energetics of the contacts and not recombination. Spies et al.[44] has identified two contributions to the reduction of V_{oc} using non-ideal contacts. Firstly, even in the case of small surface recombination currents, an effective injection barrier at the non-selective contact caused a large gradient of the Fermi level of the majority carriers. In the case of large surface recombination current, a decrease of V_{oc} due to loss of charge carrier density was also identified.

The above studies primarily focus on device architectures where the selectivity of one of the contacts (either hole or electron) is changed. It is however not known if the improvements observed at the electron and hole contacts in single interfacial layer devices are additive in dual interfacial layer devices. In other words, is there a benefit of adding an additional interfacial layer (at the opposite contact) to bulk heterojunction device when specifically focusing on V_{oc} improvement and charge carrier lifetime? Furthermore, the studies above focus typically on one type of contact material. Given the wide range of chemical composition of interfacial layers (metal oxides, polymeric conductors, polyelectrolytes), the aim of this study is to investigate the effect of interfacial layers on the V_{oc} of bulk heterojunctions with a wide variety of interfacial materials, both polymeric and metal oxide types used at the electron and hole interfaces.

The open circuit voltage of a bulk heterojunction solar cell can be described by equation 1 as suggested by Elliott et al.[43] The V_{oc} is governed by the effective gap of the organic semiconductor (E_g), the density of states distribution described by the effective slope of the tails states (σ_{eff}) and the effective in-gap charge density (N_{teff}). The effective gap of the semiconductor is approximated by the difference between the HOMO level of the polymer and the LUMO level of the electron acceptor PCBM. Based on this model, any increase in the V_{oc} in

the presence of interfacial layers may originate from i) larger σ_{eff} due to lower density and/or shallower trap state distribution at the organic layer / contact interface or in the contact material itself, ii) larger N_{eff}, which may originate from enhanced light absorption (optical cavity effect), increased charge separation (e.g. change in dielectric constant at the contacts) and / or reduced recombination.

$$V_{oc} = \frac{E_g}{q} - \frac{S_{eff}}{q}\ln\left(\frac{N_{teff}^2}{np}\right)$$

(eq. 1)

In addition, the V_{oc} can be influenced by the contact work function. If the electrode work function (either electron or hole contact) falls within the effective gap of the organic semiconductor, the open circuit voltage can be reduced due to the presence of an energetic barrier.[44] Modifying the electrode work function to match the energy levels determined by the organic semiconductor should minimize these contact induced losses.

Charge extraction techniques have been used extensively in both photo-electrochemical and organic solar cell research to assess the effect of changes in materials energy levels on the open circuit voltage.[45] A typical example is the effect of electrolyte additives, such as tert-butylpyridine or $LiClO_4$, on the open circuit voltage of dye-sensitized solar cells.[46] By adsorbing molecular or ionic compounds on the semiconductor surface, the additives can alter the potential of the bottom of the conduction band of the TiO_2, which in turn affects the V_{oc} of the device. V_{oc} versus charge density plots obtained by charge extraction and photovoltage measurements allow the comparison of V_{oc} at the same charge density. Any shift in V_{oc} at the same charge density is attributed to changes in the materials energy levels, while a change in the slope of V_{oc} versus charge density may suggest that the trap state density or trap state energy distribution has

changed.[43] Charge density decay versus time plots can be used to calculate charge carrier lifetime. Therefore, in principle, charge extraction measurements are able to separate the various effects (change in work function, trap density or recombination kinetics) of interfacial layers on the V_{oc} of organic solar cells. Charge extraction and photovoltage decay measurements are relatively simple, inexpensive and can be performed on actual device architectures.

To investigate the effect of interfacial layers on the performance of solar cells using charge extraction measurements, four type of device structures (Fig. 1.) have been prepared using the active layer consisting of poly[N - 9′-hepta-decanyl-2,7-carbazole-alt-5,5-(4′,7′-di-2-thienyl-2′,1′,3′-benzothiadiazole)](PCDTBT) :)]:[6,6]-phenyl C70-butyric acid methyl ester (PC[70]BM) (1:4) sandwiched between indium tin oxide coated glass and evaporated aluminum electrodes (reference device). PCDTBT was selected due to its relatively high oxidation potential, suggesting the open circuit voltage of the devices could be more significantly influenced by the hole contact work function.[1]
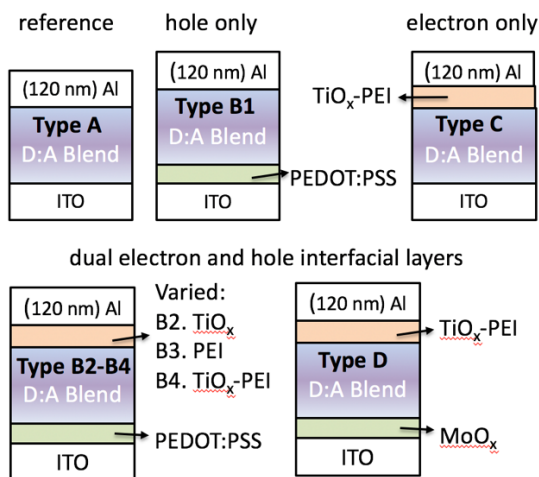

Figure 1. The types of bulk heterojunction solar cell device structures with various combinations of electron and hole interfacial layers

To cover a wider range of interfacial layers both polymer, metal oxide and polyelectrolyte types interfacial materials were selected. PEDOT-PSS and a solution processed MoO_x layer developed in house were used as a hole contact layer (B1 and D). Solution deposited TiO_x, PEI and their combination TiO_x-PEI prepared by subsequent solution deposition of PEI and TiO_x were selected as electron interfacial layers (C, B1-B4).

Type A (reference) device consists of indium thin oxide (ITO) coated glass as the hole contact and evaporated aluminum (Al) as electron contact without any additional interfacial layers; ii) type B devices consist of PEDOT-PSS as hole contact layer and the electron interfacial layers detailed in **Figure 1** (B1: no electron interfacial layer; B2: TiO_x; B3: PEI; B4: combination of TiO_x -PEI; iii) type C consists of a TiO_x-PEI electron contact layer without a hole transport layer, and iv) type D consist of a TiO_x-PEI electron contact layer and a MoO_x hole contact layer.

Current – voltage measurements under illumination and in the dark (Figure 2, 3) were performed to assess the performance of the solar cells as well as the diode rectification behavior in the dark, while external quantum efficiency (EQE) (Figure 4) were used to compare the charge collection efficiencies and the optical absorption of the interfacial layers. Photovoltage decay (Figure 5) combined with charge extraction using a nanosecond switch technique (Figure 6) were employed to determine the effect of interfacial layers on charge density versus open circuit voltage (Figure 8), whereas the decay of extracted charge at various time delays was used to calculate charge carrier lifetime versus charge density at open circuit conditions (Figure 7).

RESULTS AND DISCUSSION

Effect of interfacial layers on the device performance of bulk heterojunction solar cells using PCDTBT:PC[70]BM active layers

Table 1 shows the average values and standard variation (averaged for 8 devices) of photovoltaic parameters measured under 100 mW cm^{-2} simulated Air Mass (AM) 1.5 illumination for photovoltaic devices consisting of PCDTBT:PC[70]BM as active layers and various hole and electron contact interfacial layers. Figure 2 and 3 show current density – voltage (J-V) curves measured under illumination and in the dark, respectively, for representative devices with efficiency values closest to the average values in Table 1.

The photovoltaic performance of the devices using ITO and aluminum contacts (type A, reference) without interfacial layers is poor, with the open circuit voltage (V_{oc}) and fill factor (FF) significantly lower than expected using the PCDTBT:PC[70]BM photovoltaic blend. The shape of the JV curve is almost a straight line indicating a fill factor close 0.25. Inserting a PEDOT-PSS hole contact layer (type B1, hole only) between the ITO and the active layer increases the open circuit voltage (V_{oc}) drastically from 0.23 V to 0.82 V, and the FF from 0.26 to 0.53. The short circuit current density increases by 2.9 mA cm^{-2}, leading to an increase in the power conversion efficiency by almost an order of magnitude (to 5 %).

Inserting an electron interfacial layer PEI-TiO$_x$ (type C, electron only) between the aluminum contact and the active layer also leads to large increases in device efficiency, from a 0.23 V to 0.87 V increase in the open circuit voltage, 0.26 to 0.55 increase in FF and 1.5 mA cm^{-2} increase in the J_{sc} compared to the reference devices (A). The JV curves of the B1 and C devices show similar characteristics. Electron interfacial layer only devices (C) show a higher V_{oc} but lower J_{sc} compared to B1 (hole only).

Using a PEDOT-PSS hole interfacial layer in combination with an electron interfacial layer i) TiO_x (Type B2), ii) PEI (type B3) or iii) a TiO_x - PEI (B4) further improves the performance compared to hole only interfacial layer B1, mainly by further increasing the open circuit voltage by 50 to 70 mV. In addition, the TiO_x-PEI electron interfacial layer also improves the FF to 0.58, leading to the highest power conversion efficiency of 6% for the various combination of device architectures reported herein. The highest V_{oc} of 870 to 890 mV is obtained whenever an electron interfacial layer was present (B2 -B4, C), while the J_{sc} was the same within error for all devices using a hole interfacial layer.

Using MoO_x hole interfacial layer deposited from a water-based solution using a procedure developed in house in combination with a TiO_x-PEI electron interfacial layer (Type D) also improves the performance compared to reference device A, with slightly lower power conversion efficiency compared to using PEDOT-PSS (see B4) due to the lower FF. We note that single interfacial layer MoO_x devices using the solution deposition method developed here were not reproducible, possibly related to pinholes and the difficulty to control the thickness and quality of the thin MoOx film. In dual interfacial layer devices, the presence of the additional electron interfacial layer rectified these issues with reproducibility suggesting the pinhole type defects in the hole interfacial layer can be rectified by adding an electron interfacial layer.

The above results confirm the well-known benefits of using interfacial layers with large increases to the performance of devices. It does not seem to significantly matter in terms of photovoltaic performance whether an electron or hole interfacial layer is used, as long as the selectivity of one of the contacts is improved. The combination of two interfacial layers bring the most benefits by further increases to the V_{oc}, but clearly, the V_{oc} increase obtained in single (hole only or electron only) interfacial devices compared to the reference device A are not additive.

Due to the non-additive nature of the effects of interfacial layer in dual interfacial layer devices, the results cannot be simply explained by a better aligned work function at the electron and hole side and the effect of change in charge carrier lifetime needs to be also considered.

Figure 3 shows the J-V curves recorded in the dark for representative photovoltaic devices on a logarithmic scale. Device type A without additional interfacial layers shows the highest current and almost no difference between the negative and forward bias currents with poor diode rectification. Inserting a hole interfacial layer (PEDOT-PSS (B1)) leads to three orders of magnitude reduction in the reverse bias current and a distinct diode behavior. Inserting an electron interfacial layer (PEI-TiO$_x$ (C)) also reduces the reverse bias current with the diode rectification similar compared to B1. However, the injection onset voltage (determined from the intersection of two lines of the high and low current regimes in forward bias in a semilog plot) is shifted to more positive potentials by approximately 70 mV. Generally, the reverse bias currents measured for type C devices were unstable, showing step-like decreases in the current when swept from lower to higher reverse bias. This can be attributed to the presence of device shunts and pinholes, possibly due to the roughness of the ITO interface. The dark current measured for devices with hole interfacial layers did not exhibit such behavior suggesting that one of the functions of the hole interfacial layers is to smooth the surface of the ITO preventing the shorting of the device through pinholes. Devices with the highest photovoltaic performance (Type B4) show the lowest reverse bias currents, the highest forward bias currents and the largest onset potentials. Devices using TiO$_x$ electron interfacial layers either with or without the PEI showed the highest injection onset potentials, while PEI electron interfacial layer alone (B3) did not change the injection onset as compared to the device B1. Devices using MoO$_x$ (D) show higher

reverse bias current compared to type B2 and B4, suggesting that the MoO_x layer employed in these studies is not as effective a blocking contact as PEDOT-PSS.

Note that the JV curves selected here were representative of the devices prepared. However, a large variation in the dark current behavior was observed within the same device structure despite the fact that their performance under illumination was quite reproducible (See Supporting Information S1 and S2). The large variation in the reverse bias currents in the dark current-voltage measurements suggest the presence of pinholes which mainly determine the reverse bias dark current. A few tens of μA cm^{-2} leakage current through pinholes can dominate the reverse bias current, however, under illumination, the effect of leakage current is not so significant with photocurrent densities in excess of 10 mA cm^{-2}. In the presence of pinholes, it is difficult to predict how much of the dark current is due to recombination current at the particular interfacial layer used, therefore analysis of the recombination behavior based on dark current-voltage measurements in this case is uncertain.

To further investigate the origin of the difference in J_{sc} between hole and electron interfacial layer devices, external quantum efficiency (EQE) spectra of solar cell devices fabricated using various interlayers have been determined (**Figure 4**). The predicted short circuit currents under 100 mW cm^{-2} white light illumination (Table 1, Calculated J_{sc})) are obtained by integrating the EQE spectra with the AM 1.5 spectrum. The calculated J_{sc} of devices A and C is almost identical to the values measured by calibrated white light illumination. However, the calculated J_{sc} of devices containing PEDOT-PSS or MoO_x hole contact layers (B1 – B4, D) is approximately 10% lower than obtained by calibrated white light illumination. The device without interfacial layer (type A) shows an EQE peak at 380 nm and a broad maximum at 560 nm with EQE values reaching 57% and 54%, respectively. Adding a PEDOT-PSS hole interfacial layer (Type B1)

increases the EQE values by over 10% without any changes to the shape of the spectrum. Inserting a PEI-TiO$_x$ electron interfacial layer (Type C) results in a blue-shifted EQE spectrum, with the first peak 5% lower than that of type B1 (Fig. 4 A). Using electron interfacial layers in combination with PEDOT- PSS hole interfacial layers (B1 – B4, Fig. 4 B) results in only small (< 5%) changes to the magnitude or shape of the EQE spectra. Using MoO$_x$ instead of PEDOT in combination with the PEI-TiO$_x$ electron interfacial layer (Type D) results in a slightly blue shifted and decreased first EQE peak near 400 nm, and lower values at the red-edge of the spectrum.

The most significant difference in the J_{SC} measured under white light (Table 1) of the devices is the 10% lower J_{SC} using an electron interfacial layer (C) compared to hole interfacial layer (PEDOT-PSS or MoO$_x$, B1 or D). This could be attributed to an optical interference effect due to the different layer stack. However, EQE measurements show only minor peaks shifts with the interfacial layers used. The J_{sc} obtained by integrating the EQE is quite similar between electron and hole interfacial layer devices, which suggests that the higher J_{sc} measured under white light illumination is attributed to a measurement error due to a stray photocurrent response from outside of the geometric area defined by the overlap of ITO and aluminum contacts when highly conductive PEDOT-PSS or MoO$_x$ hole interfacial layers are used (type B1-4, D). The stray photocurrent is evident from the consistently larger J_{sc} measured for PEDOT-PSS or MoO$_x$ containing devices (100 mW cm^{-2} white light illumination) as compared to EQE measurements, where the monochromatic light was focused inside the device active area. Similar effects have been reported in the literature by Cravino et al. and were attributed to the large conductivity of the PEDOT-PSS increasing the charge collection area beyond the geometric area of the device.[47] A blue shift of the EQE spectrum in case of the electron interfacial layer only device (C) could be

explained by a change in the layer stack of the device causing different coupling of light in the optical cavity formed between the front and back electrodes. The thickness of the PEDOT-PSS is between 30 and 40 nm, which could shift the optical field in the device enhancing light absorption towards the red part of the spectrum.[48] However, such optical cavity effects do not contribute significantly the change in the photocurrent. The EQE peak at 380 nm is also blue shifted in the case of MoO_x interfacial layer devices. The MoO_x layer used in this work was highly transparent in the UV-vis spectrum range (the transmission of the ITO coated glass was not changed after the deposition of the MoO_x layer, not shown), further confirming that the use of thicker PEDOT-PSS layer may be the origin of the red shifted spectrum in the EQE in B type devices.

The effect of interfacial layers on charge recombination

Figure 5 shows photovoltage transients obtained by illuminating the solar cell devices with 6 to 8 ns laser pulses at 532 nm and at laser intensities corresponding to the saturation of the photovoltage signal magnitude. The photovoltage transient of the reference device without interfacial layers (Type A) decays within tens of microseconds and shows the lowest initial photovoltage value of 0.57 V. Inserting a PEDOT:PSS interfacial layer (B1) leads to an increase in the initial photovoltage value to 0.74 V and extends the decay to the several tens of milliseconds time scale. A 4% rise in the voltage signal magnitude peaking at 4 µs and at 0.77 V is observed. Inserting an electron interfacial layer PEI-TiO_x (C), results in the same initial voltage magnitude (0.74 V) compared to B1 and a rise signal peaking at 0.83 V. The observed photovoltage decay is slightly faster compared to that of B1 (Fig. 5 A).

Inserting both a TiO_x electron interfacial layer and a PEDOT-PSS hole interfacial layer (Type B2, Fig. 4 B) increases the initial voltage to 0.82 V. The transient exhibits a rise to 0.84 V within

1 μs and a similar decay on the millisecond time scale to B1. Using PEI as the electron interfacial layer (type B3) results in a larger initial voltage value of 0.88 and no photovoltage rise is observed. Using a combination of TiO_x - PEI electron interfacial layer (type B4) results in a similar initial voltage value compared to type B3 with no voltage rise and the longest voltage decays recorded among the various type solar cells. Replacing PEDOT-PSS with MoO_x layer results in an order of magnitude faster voltage decay with maximum voltage values marginally higher than measured for B4 type devices. When compared to device C, the addition of an MoO_x layer accelerates the photovoltage decay by almost an order of magnitude, which could indicate faster recombination at the ITO-MoO_x hole interface as compared to the bare ITO electrode.

The photovoltage decays measured with short laser pulses represent the time dependence of eq. 1 with the possible influence of i) the variation in charge density due to either charge migration inside the device (external current minimized by using a high impedance) or recombination; (ii) change in the midgap density of states occupation $d\sigma_{eff}/dt$ due to energy relaxation of charge carriers within the DOS following the initial charge generation step. Note that the photovoltage decay measurements were recorded using a 1 MOhm impedance, set by an oscilloscope. Therefore the decays measured towards the millisecond timescale could be influenced by current through the RC circuit, rather than recombination internally in the device. Therefore the measured curves are compared from the sub-microsecond to 1 ms time scale.[49] The much higher transient photovoltage values for the reference device A compared to the steady state measurements (0.26 V) suggest higher charge density, at least initially, in transient measurements compared to what is achievable under AM 1.5 illumination. The photovoltage rise (measured for B1, B2 and C) suggest inhomogeneous charge distribution at early times with at least of one of the charge carriers migrating to the contacts on the microsecond time scale. No

16

voltage rise was observed in dual interfacial layer devices or reference device A suggesting that any spatial charge separation in the device (for example from bulk towards to the contacts) occurs faster than in single interfacial layer devices. The difference in the magnitude of V_{oc} values with various interfacial layers could be due to differences in the work function of the electrode influencing the energy level alignment, or differences in charge density due to differences in recombination lifetime. However, the time scale of the photovoltage decay is influenced by charge recombination as well as the time dependent occupation of the midgap states. To separate the two effects, charge extraction measurements using a nanosecond switch were employed.

Figure 6 shows charge carrier density decays as a function of delay times obtained by a charge extraction method. The devices were photoexcited at 532 nm at the same laser intensity as above, while held at open circuit condition using a nanosecond switch (2.2 MΩ impedance). After an adjustable delay time, the impedance of the switch was changed to 50 Ω resulting in the extraction of charges from the device. The charge densities were obtained by integrating the photocurrent transients. The measured charge density decreases with increasing delay time due to recombination. The reference device without additional interfacial layers (type A, Fig. 6 a)) shows the lowest initial charge densities (5×10^{16} cm^{-3}), and the fastest charge density decays. Adding a PEDOT-PSS layer (B1) increases the initial charge density to 9.0×10^{16} cm^{-3} and slows down the decay kinetics. Inserting a PEI-TiO$_x$ electron interfacial layer (C) results in slightly lower charge density values, and similar decays (until the millisecond time scale) when compared to devices with type B1.

Up to 50 microsecond delay times, the charge density decays are very similar for B1 to B4 devices (Fig. 6 B). Device B1 and D show 20% lower extracted charge density compared to B3

and B4 within this timescale. Beyond 50 microseconds, B4 device shows the slowest decay, followed by B1, B3, and B2. Note that the RC decay of the electrical circuit including the switch in its open state is around a few milliseconds, therefore the long-term decays beyond a few millisecond are possibly influenced by leakage current through the RC circuit. The faster decays in B2, B3 and D can be attributed to lower shunt resistance in these devices at lower charge densities / longer delay times, attributed to the quality of the contacts including the effect of defects and pinholes. The micro to millisecond decays are the slowest for dual interfacial layer device with PEI-TiO$_x$ (B4), which also showed the largest rectification ratio in the dark JV measurements.

Figure 7 shows charge carrier lifetime calculated as a function of charge density obtained by charge extraction measurements. Note that the lifetime was calculated using eq. 2 from the *slope* of charge density decay over time, susceptible for a substantial error. The charge carrier lifetime calculated at a relatively high charge density (5×10^{16} cm^{-3}) for each device types is shown in Table 1. This charge density value was chosen because i) it is beyond the region where photovoltage rise was observed and thus minimises the impact of charge migration, ii) encompasses the measurement range for all device types, therefore comparison of the lifetime at the same charge density is possible, iii) faster than the time window where charge leakage through the RC circuit or shunt resistance may have an influence. Furthermore, by comparing five experimental techniques including transient absorption spectroscopy, impedance spectroscopy, transient photovoltage (TPV) and charge extraction using a switch and photo-CELIV, we have shown that all these method yield comparable lifetime values at this higher charge density range.[50]

The charge carrier lifetime calculated for the type A reference device without additional interfacial layers (Fig. 7 A) is just few microseconds at all charge densities measured. Inserting a PEDOT-PSS hole interfacial layer (B1) leads to 1 to 2 orders of magnitude longer charge carrier lifetime (20 μs). Inserting an electron interfacial layer (TiO$_x$-PEI, C) has a similar effect to B1, with slightly longer lifetimes determined at the same charge density. The calculated charge carrier lifetimes of device B2 are slightly shorter than the device B1. However, the calculated lifetimes slightly increase when PEI and hole interfacial layer are used (B3) compared to single interfacial layer device (B1) or (C) devices (Fig. 7 B and Table 1). The charge carrier lifetime measured using MoO$_x$ hole contact layers (D) are similar to type B1 and C devices at high charge densities. At lower charge densities corresponding to longer delay times in the charge extraction measurements, charge carrier lifetimes are longest for B1 and B4 devices whereas B2 and D devices show two orders of magnitude shorter lifetimes. Similar to the photovoltage decay measurements presented above, the shorter lifetime measured for device D compared to C could suggest that the addition of the in-house developed MoO$_x$ layer leads to faster recombination or lower shunt resistance compared to the bare ITO layer alone.

The effect of interfacial layers (except the MoO$_x$) significantly reducing recombination as a main influence on device photovoltage is confirmed by charge extraction measurements. Increasing the selectivity of one contact is sufficient to increase charge carrier lifetime (Fig. 7 A) and it does not matter greatly whether it is the electron or the hole contact interface, as long as at least one of them is modified. The device using a bare ITO electrode with an electron interfacial layer (C) has similarly long lifetime to the hole interfacial layer only device, suggesting there is nothing inherently wrong with the bare ITO electrode in terms of recombination. Compared to single interfacial layer devices, using both an electron and hole interfacial layers does not (within

the measurement error) increase the charge carrier lifetime. If surface recombination was primarily caused by recombination centers introduced by the contacts in the reference device, the above results are counterintuitive. To obtain long lifetimes, both the active layer / Al and active layer / ITO interfaces would need to be passivated by interfacial layers. This is clearly not the case as passivation of one of the interfaces is sufficient. The in-house develop MoO_x layer is different to the above as it does seem to accelerate recombination compared to using a bare ITO alone (C vs D device). Instead of the surface passivation mechanism discussed above, the reduced recombination using PEDOT-PSS / and various electron interfacial layers is suggested to originate from the spatial charge separation of electrons and holes near the contacts, induced by the increased built-in electric field. Previous applied-bias and active layer thickness dependent charge extraction measurements suggested a similar mechanism.[49] Charge carrier lifetimes in devices with thinner active layers were longer. In addition, charge carrier lifetimes in devices with thicker active layers were dependent on the applied bias magnitude, with larger applied bias leading to longer lifetimes. Those results were explained by a charge redistribution due to the internal field (larger in thinner devices or with applied bias) leading to less spatial overlap of electrons and holes leading to less recombination. The mechanism for increased lifetime with interfacial layers can also be explained by an increased built-in field due to work function modification of the contacts. Modifying at least one of the interfaces is necessary for the enhanced spatial separation, but it does not matter significantly whether it is the electron or hole interface. Spatial charge separation is indicated on the microsecond timescale in photovoltage transients as a voltage rise, observed in single interfacial layer devices B1, C (and to some extent, B2). Note that no corresponding increase in the extracted charge density was measured on the same timescale so the overall charge density did not increase. Due to redistribution near the

contacts, the local concentration of electrons and or holes near the contact regions increased causing the rise of the voltage on the same timescale.

The effect of interfacial layers on energy level alignment (V_{oc} versus charge density)

Figure 8 shows the open circuit voltage versus charge density obtained by combining the results from charge extraction and photovoltage decay measurements. Fig. 8 (A) clearly shows increased V_{oc} at the same charge density between type A, C and B1 devices. The effective trap density (σ_{eff}), indicated by the different slope of V_{oc} versus charge density also changed, especially for the B1 type device showing a faster decay at lower charge density. The slope of dV_{oc} / dn is the smallest whenever a metal oxide layer (TiO$_x$ as electron interfacial layer or MoO$_x$ as hole interfacial layer) is used, which suggests a broader distribution of the effective density of states near the electron contact. This is consistent with the observation of electron trapping in solution processed metal oxides with a broad distribution of electron (hole) trap states located below (above) the band edges.[51] Since the same active layer blend is used, we do not expect the organic semiconductor effective bandgap to change, although the change of the surface morphology / composition of the active layer due to the deposition of the interfacial layer cannot be ruled out. The general observation of using metal oxide interfacial layers at either the hole (before active layer deposition) and electron (following after layer deposition) suggest a general property of the metal oxide layer and not a deposition induced effect.

At high charge density and early delay times in the charge extraction measurements, which corresponds to the saturation of the photovoltage signal, the slope of V_{oc} versus charge density is smaller, and the observed shift along the y axis suggest a change in the Fermi level at the contacts at the same charge density. From the photovoltage at a constant charge density of

6×10^{16} cm^{-3}, the open circuit voltage gains ΔV_{oc} due to changing the effective injection barrier can be estimated. The V_{oc} of devices at the same charge density is B1 = 0.78 V, C = 0.86 V and A = 0.57 V (Table 1). The V_{oc} increase at the hole contact due to lowering of the effective injection barrier using PEDOT-PSS is calculated as $\Delta V_{oc}{}^h = V_{oc}(B1) - V_{oc}(A) = 0.21$ V, while the V_{oc} increase at the electron contact side attributed to the PEI-TiO$_x$ interfacial layer is $\Delta V_{oc}{}^e = V_{oc}(C) - V_{oc}(A) = 0.29$ V. When comparing with the steady state open circuit voltages obtained under 100 mW cm^{-2} white light illumination (Table 1), the most significant difference between the measured steady state and transient photovoltage values is the lower steady state $V_{oc}{}^{st}$ obtained using type A devices. This difference can be clearly attributed to the lower charge density under steady state conditions due to fast recombination (Fig. 7). In charge extraction measurements, much higher charge densities can be obtained at early delay times and stronger laser intensities than under steady state illumination. For the other devices, the difference between the V_{oc} obtained under steady state illumination and in charge extraction measurements at constant charge density is between 5 to 40 mV, which is similar to the error bar of the V_{oc} measurement under steady state conditions. A further contribution may arise from a different charge distribution in the device or a different trap state occupancy under steady state conditions as compared to time-resolved measurements. [45, 52]

Assuming that the photovoltage increases, due to charge density increase and the change of work function, are additive under steady state illumination, the photovoltage increase due to reduced recombination in device B1 can be calculated as $\Delta V_{oc}{}^{rec} = V_{oc}{}^{st}(B1) - V_{oc}{}^{st}(A) - \Delta V_{oc}{}^h = $ 0.82 V $-$ 0.23 V - 0.21 V = 0.38 V, and for electron interfacial layer device C is $\Delta V_{oc}{}^{rec} = V_{oc}{}^{st}(C) - V_{oc}{}^{st}(A) - \Delta V_{oc}{}^e = $ 0.87 V $-$ 0.23 V- 0.29 V= 0.35 V. The good agreement between the $\Delta V_{oc}{}^{rec}$ values obtained independently for electron and hole interfacial layer devices is consistent

with the very similar electron lifetime measured (hence similar charge density as steady state illumination) for B1 and C devices.

The above calculations qualitatively demonstrate that the most significant effect of using either an electron or hole interfacial layer compared to the bare ITO and Al electrodes is the increased V_{oc} due to reduced recombination ($\Delta V_{oc}^{rec} \sim 0.38$ V), with additional benefits attributed to the better aligned electrode work functions ($\Delta V_{oc}^{h} = 0.21$ V, $\Delta V_{oc}^{e} = 0.26$ V). A PEDOT-PSS hole interfacial layer provides the same benefits in terms of reducing recombination to PEI-TiO$_x$, however, the V_{oc} increase due to lowering of the effective injection barrier at this interface is less than at the electron contact.

The question arises why the increases in photovoltage due to work function alignment at the hole and electron interface are not additive in dual interfacial layer devices? If they were, the V_{oc} was expected to further increase by at least 0.2 V to above 1 (V_{oc}^{st}(B1) $+\Delta V_{oc}^{e} = 0.82$ V + 0.29 V = 1.11 V or V_{oc}^{st}(C) $+ \Delta V_{oc}^{h} = 0.87$ V + 0.21 V = 1.08 V. The steady state V_{oc} of dual interfacial layer devices B4 has improved as compared to single interfacial layer devices, but only by 20 mV (electron only) to 70 mV(hole only) to 890 mV (Table 1). One possibility for the lack of further V$_{oc}$ increase is that the work function of PEDOT-PSS is altered during the solution deposition of the electron interfacial layer PEI-TiO$_x$, due to, for example the solvent penetrating the active layer and interacting with the PEDOT-PSS layer (ΔV_{oc}^{h} is less than in single layer devices). The effect of solvent treatment on the work function of PEDOT-PSS is well known.[53-54] However, we did not find any change in the V_{oc} of the single interfacial layer device when the isopropyl alcohol : water (the solvent used for depositing the PEI-TiO$_x$ layer) was deposited on top of the active layer, suggesting that the work function of PEDOT-PSS is not altered during the deposition of the PEI-TiO$_x$.

We propose the reason for the V_{oc} not increasing additively in dual interfacial layer devices is the lack of further increase in charge carrier lifetime and thus no further increase in charge density. In the absence of interfacial layers (reference device A), the built-in field is small and therefore the overlap of electron and hole population is large, leading to fast recombination on the microsecond time scale. By adding one interfacial layer, either electron or hole, the built-in field increases leading to charge separation in the device and reduced overlap between electrons and holes. This leads to 1 to 2 orders of magnitude longer lifetime, increased charge density and consequently, increased Fermi level at the contacts. Adding a second interfacial layer does not lead to any further charge separation and therefore the lifetime does not increase substantially. Because of this, the charge density does not increase substantially at the contacts and therefore the V_{oc} increases only marginally.

The effective bandgap E_g in eq. 1 has conceptually the same meaning as the CT state energy E_{CT}, which has been determined experimentally for the PCDTBT:PC$_{71}$BM blend.[55] Ultraviolet photoelectron spectroscopy (UPS) and charge modulated electroabsorption spectroscopy (CMEAS) measurements yielded values of 1.45 and 1.32 eV for E_{CT}, respectively. The zero kelvin V_{oc}, which represents the maximum achievable V_{oc} in the absence of bimolecular recombination according to Eq. 1, was determined to be 1.35 V. A V_{oc} loss of 0.4 V at room temperature was attributed to recombination as well dielectric loss required to overcome the coulomb interaction of the electron or hole pair in the CT state. The results herein suggest that the built-in field even in dual interfacial layer devices is not sufficient to significantly reduce bimolecular recombination losses to V_{oc}, hence the V_{oc} reaches the room temperature limit.[56]

CONCLUSION

The aim of this work was to investigate the effect of interfacial layers on the photovoltaic performance of bulk heterojunction solar cells using charge extraction measurements, with a particular focus on understanding the origin of V_{oc} change. To this end, four types of devices, with and without electron and hole interfacial layers, as well as devices employing both electron and hole interfacial layers were fabricated. The beneficial effects of interfacial layers were confirmed by large increases to the J_{sc}, V_{oc} and FF of the devices compared to the reference device, with the best photovoltaic performance of 6% obtained using a PEDOT-PSS hole interfacial layer and a combination of polyethoxylate imine (PEI) and TiO_x electron interfacial layer. The increase in the J_{sc} was partially attributed to charge collection outside the geometric active area when a conductive hole interfacial layers was used. An important finding is that no significant difference in V_{oc} and lifetime was found between single interfacial layer devices (electron or hole) and dual layer interfacial layer devices suggesting there is nothing inherently wrong with the ITO or aluminum interface in terms of recombination. An explanation based the larger spatial redistribution of electrons and holes towards the contacts due to an increased internal electric field was presented. Such charge redistribution is expected to reduce the probability for electron and hole recombination. In dual interfacial layer devices, the V_{oc} increases observed in single interfacial layers devices were not additive, which was explained by the lack of further improvement in charge carrier lifetime and consequently, no further increase in charge density near the contacts. Using V_{oc} values determined at the same charge density, V_{oc} increases due to reduced recombination and work function change at the contacts could be estimated. The methodology presented here should guide the development of interfacial layers with improved properties (example of a solution processable MoO_x layer is presented) and should help our understanding of the V_{oc} limitations due to contacts in organic solar cells. The results suggested that the in house developed MoO_x may

accelerate recombination as compared to bare ITO device when the same electron interfacial layer was used.

EXPERIMENTAL SECTION

Materials

PEDOT:PSS 0.8%w/V (Al 4083, Heraeus Precious Metals GmbH & Co. KG) was diluted with isopropanol at 1:1 ratio and shaken with orbital shaker for 30 minutes. The PEDOT:PSS film was deposited using spin coating at 5,000 rpm for 40 s.   The PEDOT-PSS layer was annealed at 150 ^{0}C for 15 min in air.

MoO$_x$ precursor solution was prepared by dissolving 150 mg molybdenum (VI) oxide (Sigma-Aldrich) in 1 ml of 30% ammonium hydroxide to prepare a stock solution. Prior to deposition, the stock solution was diluted with deionized water to give a concentration of Molybdenum oxide at 6 mg/ml respectively. The solution was deposited by spin coating at 8,000 rpm for 40 s, and then the films were heated to 150^{0}C for 20 minutes. The thickness of the films could not be determined.

TiO$_x$ interfacial layer was prepared by a sol-gel route.[57] A precursor solution containing 1 ml titanium diisoporpoxide bis(acetonate) 75% in isopropanol was diluted in 8 ml isopropanol and stirred. 0.5 ml glacial acetic acid was added, followed by 0.5 ml of deionized water. The solution was heated to 60 ^{0}C and kept overnight. Prior deposition, the titanium oxide stock solution was diluted with isopropanol at 1 to 6 volume ratio before depositing on top of the active layer by spin coating at 5000 rpm for 40 s.

50% w/v of **PEI** (MW 750,000, Sigma-Aldrich), was diluted with 2-methoxyethanol to get 0.5

w%/V PEI solution. This solution was deposited on top of the active layer by spin coating at

5000 rpm for 40 s.

TiO$_x$-PEI bilayer was prepared by spin coating the PEI layer on the top of TiO$_x$ layer

following the deposition conditions above.

Device fabrication

ITO substrate (Xin Yan Technology Limited) was cleaned by ultra-sonication in washing

detergent, deionized water, acetone and isopropanol, for 15 minutes each steps; followed by UV-

Ozone treatment for 15 minutes. The photoactive layer, either on top of hole contact interfacial

layer, or on ITO, was deposited by spin coating a solution of PCDTBT (7 mg/ml) and PC[71]BM

(28 mg/ml) dissolved in 1,2-dichlorobenzene (o-DCB) at 1100 RPM. A 120 nm thick aluminum

was thermally evaporated at < 10^{-6} mbar either directly on top of the active layer or following the

deposition of an electron interfacial layer. Devices were encapsulated using a UV epoxy resin in

an argon-filled glove box. Current density–voltage (J–V) characteristics were measured under air

mass 1.5G solar illumination (100 mW cm^{-2}) by using a Keithley 2400 source measurement unit.

External quantum efficiency (EQE) spectra and internal quantum efficiency (IQE) were

measured using an EQE system (PV measurement, model QEX10).

Time-Resolved Charge Extraction using a nanosecond switch measurements were performed

as described in the literature. [14, 49 - 50, 58-59] The encapsulated devices were connected to a switch

(Asamama Lab solar relay, 2.2 Mohm impedance when open) and photo-excited by a Nd:YAG

laser (Spectra-Physics, INDI-40-1, 532 nm, 10 μJ cm^{-2} and 10 Hz repetition rate). After an

adjustable time delay controlled by a delay generator, the switch is closed (250 ns, less than 50-

ohm impedance) resulting in a current transient, recorded by a digital oscilloscope (Tektronics,

DPO4054) at 50 Ω impedance. The dark capacitive and switch noise response were subtracted to obtain photocurrent transient. Integration of the photocurrent transient yield the number of charges, and charge density was calculated by dividing the number of extracted charges by the active layer film volume. Charge carrier lifetime (τ) was calculated from charge density decay using equation 2.

$$t = -n \left(\frac{dn}{dt} \right)^{-1} \tag{2}$$

Where, n and t are the charge carrier density and delay time respectively.

For **photovoltage decay measurements**, the device was connected to the same oscilloscope as above while illuminated by a laser pulse with the same intensity as above. The voltage transient was recorded using a 1 MΩ impedance. To create the voltage – charge density plot, the voltages from photovoltage decay measurements were plotted versus the extracted charge at matched delay times obtained in the charge extraction measurement.
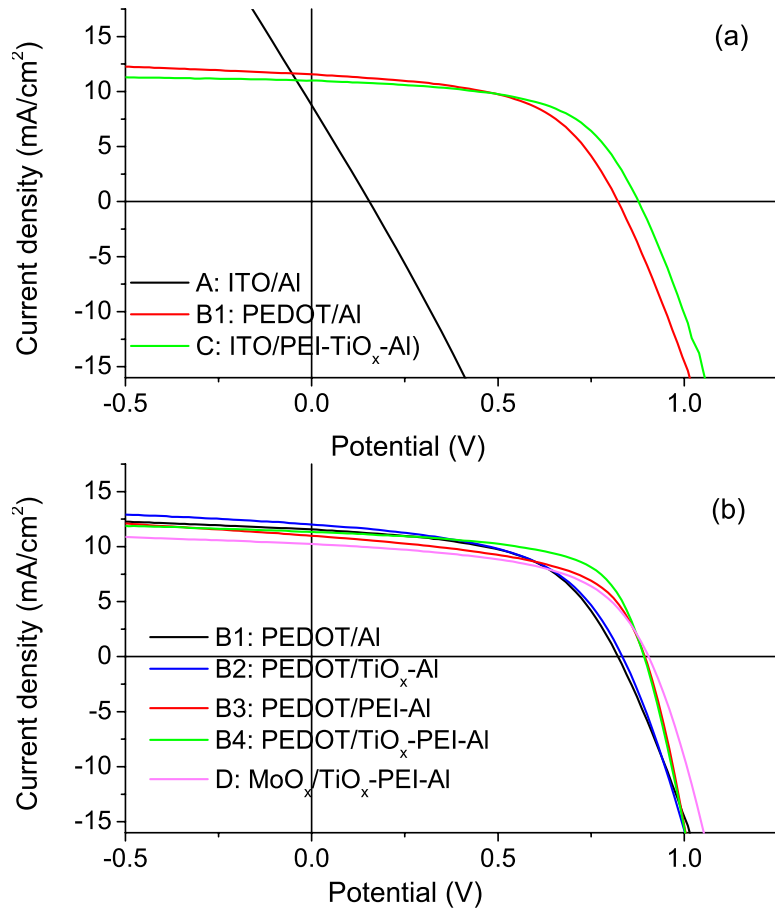
FIGURES

Figure 2. Current – voltage curves recorded under calibrated AM 1.5 100 mW cm^{-2}

illumination with various interfacial layers, (a) Current – voltage curves of device type A, C and

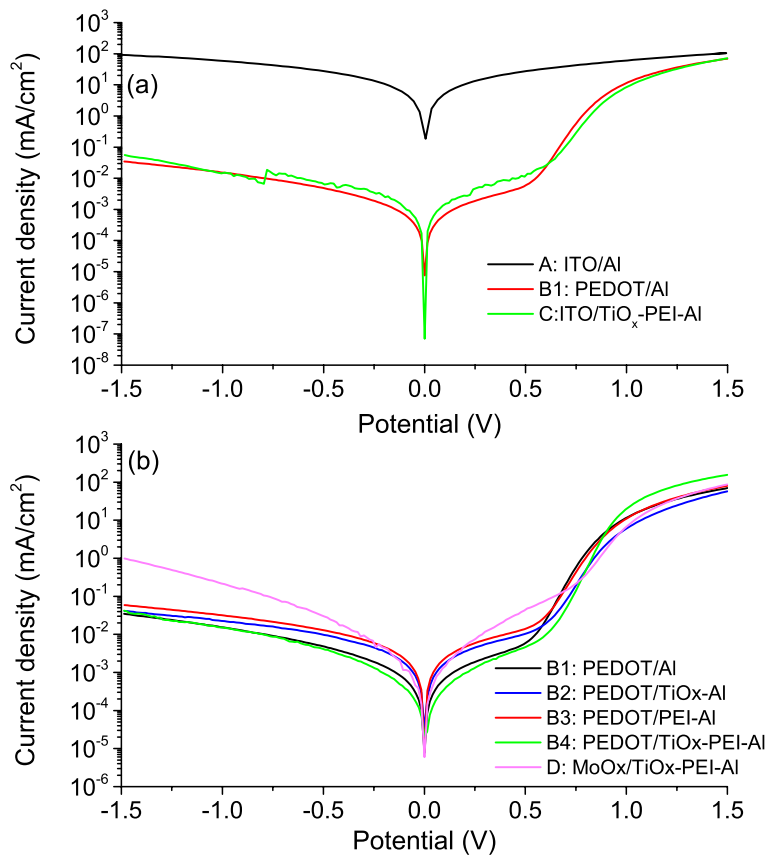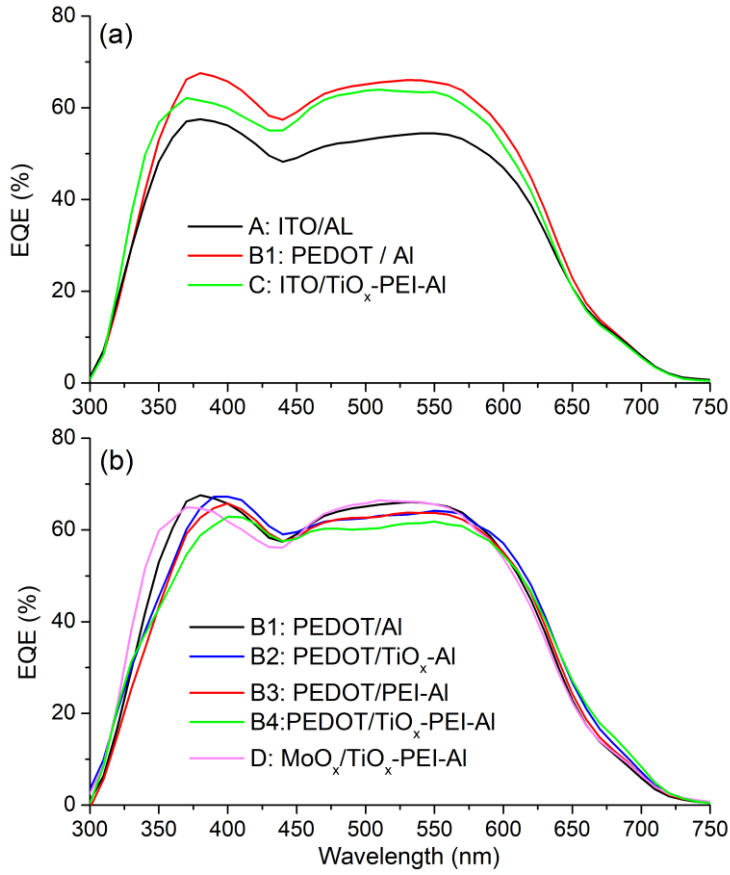B1, (b) Current – voltage curves of device type B1, B2, B3, B4 and device type D

Figure 3. Current density – voltage curves recorded in the dark for devices utilizing various interfacial layers, (a) Current – voltage curves of device type A, C and B1, (b) Current – voltage curves of type B1, B2, B3, B4 and type D device.

Figure 4. External quantum efficiency (EQE) for devices utilizing various interfacial layers, (a) EQE of device type A, C and B1, (b) EQE of type B1, B2, B3, B4 and type D device.
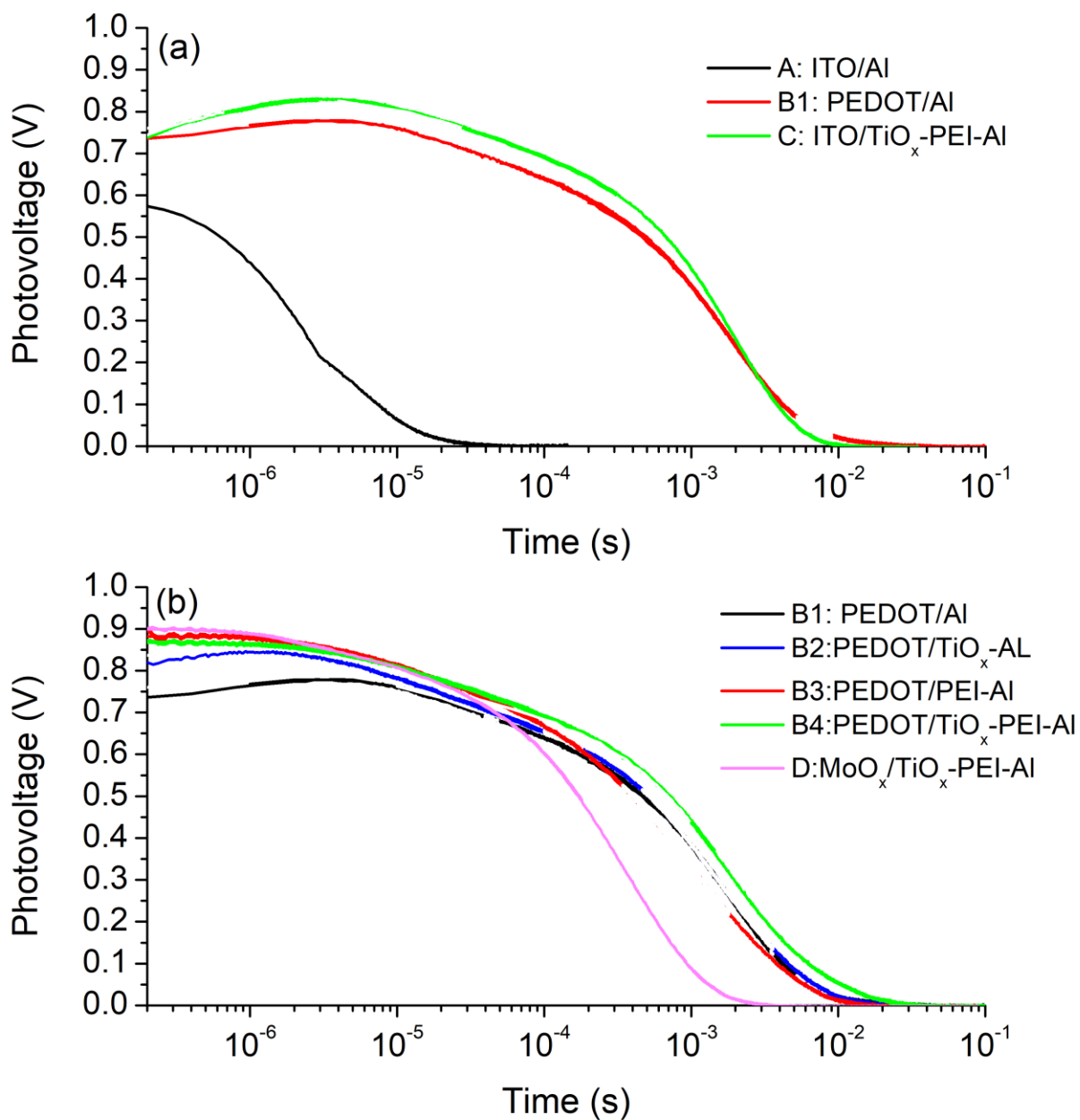
Figure 5. Photo-voltage decay transients recorded for photovoltaic devices utilizing various interfacial layers, (a) Photo-voltage decay transients of device type A, C and B1, (b) Photo-voltage decay transients of device type B1, B2, B3, B4 and type D.
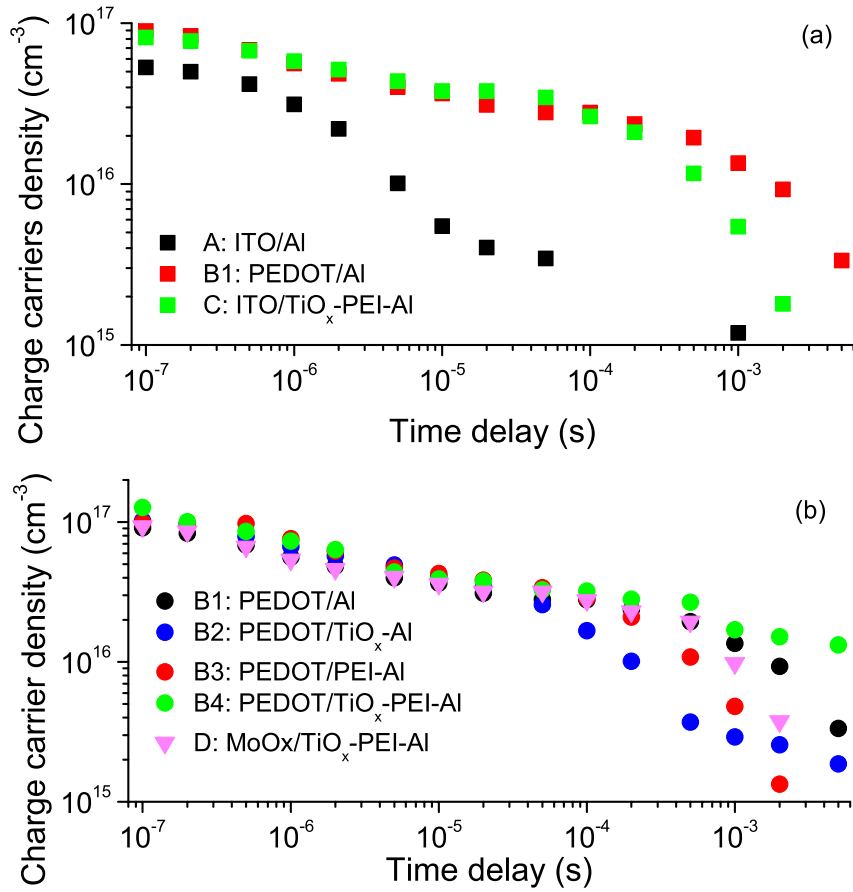
Figure 6. Charge carrier density decay as a function of delay time recorded for photovoltaic devices utilizing various interfacial layers, (a) Charge carrier density decay as a function of delay time of device type A, C and B1, (b) Charge carrier density decay as a function of delay time of device type B1, B2, B3, B4 and type D.
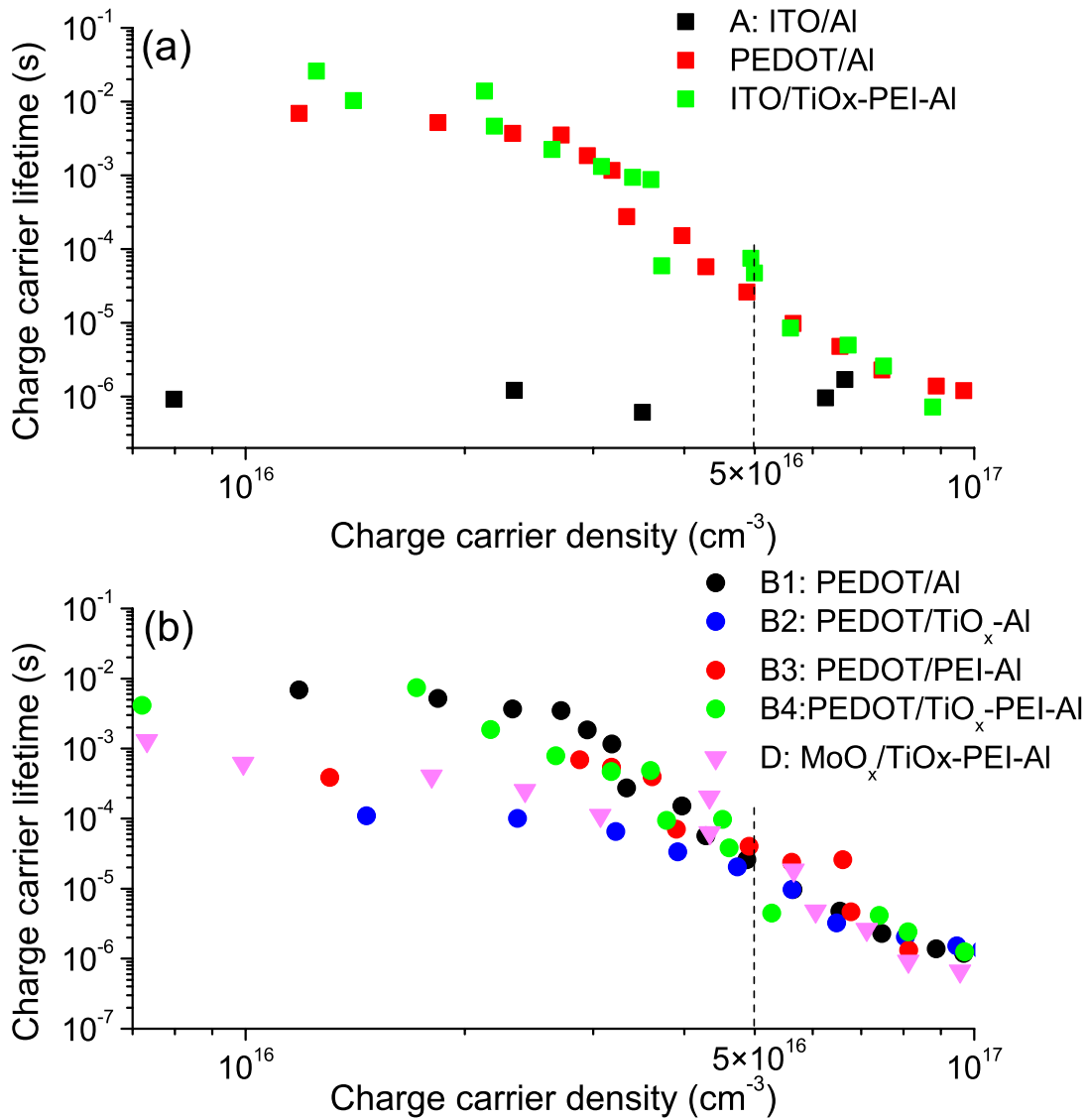
Figure 7. Charge carrier lifetime as a function of charge carrier density for photovoltaic devices utilizing various interfacial layers, (a) Charge carrier lifetime as a function of charge carrier density of device type A, C and B1, (b) C Charge carrier lifetime as a function of charge carrier density of device type B1, B2, B3, B4 and type D.
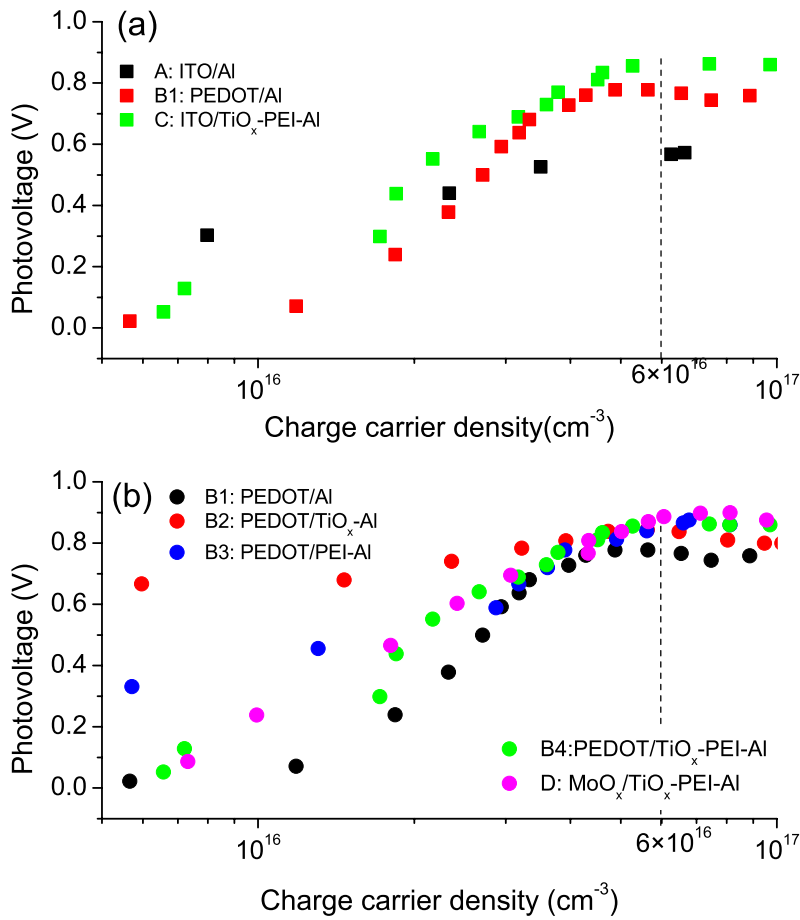
Figure 8. Voltage versus charge carrier density measured by photovoltage decay and charge extraction measurements, (a) Voltage versus charge carrier density measured by photovoltage decay and charge extraction measurements of device type A, C and B1 devices, (b) Voltage versus charge carrier density measured by photovoltage decay and charge extraction measurements of device type B1, B2, B3, B4 and type D.

TABLES.

Table 1. Photovoltaic performance, calculated short circuit current (J_{sc}), Charge carrier lifetime and V_{oc} at fixed charge density determined for PCDTBT:PC[70]BM (1:4 ratio) solar cell devices fabricated using various interfacial layers

Device type	Interfacial layer		Average photovoltaic parameters				Calculated J_{sc} (mA cm^{-2}) from EQE	Charge carrier lifetime (s) at 5×10^{16} cm^{-3}	V_{oc} (mV) at 6×10^{16} cm^{-3}
	Hole	Electron	V_{OC} (mV)	J_{sc} (mA cm^{-2})	FF	PCE (%)			
A	w/o	w/o	230±80	8.6 ± 0.7	0.26±0.01	0.5 ± 0.2	8.5	1.7 µs	570
B1	PEDOT-PSS	w/o	820±20	11.5±0.7	0.53±0.04	5.0±0.5	10.6	20 µs	780
B2	PEDOT-PSS	TiO$_x$	870±30	11.8±0.4	0.52±0.02	5.3±0.02	10.3	14 µs	845
B3	PEDOT-PSS	PEI	880±20	11.2±0.6	0.53±0.06	5.2±0.8	10.2	39 µs	855
B4	PEDOT-PSS	TiO$_x$ - PEI	890±10	11.1±0.6	0.58±0.05	6.0±0.7	10.2	22 µs	875
C	w/o	TiO$_x$ - PEI	870±20	10.1±1.0	0.55±0.05	4.9±0.8	10.2	33 µs	860
D	MoO$_x$	TiO$_x$ - PEI	890±20	11.1±0.6	0.51±0.08	5.0±0.7	10.2	24 µs	880

ASSOCIATED CONTENT

Supporting Information. Device-to-device variation of current – voltage curves with various interfacial layers recorded under calibrated AM 1.5 100 mW cm^{-2} illumination (S1) and in the dark (S2). This material is available free of charge via the Internet at http://pubs.acs.org.

AUTHOR INFORMATION

Corresponding Author

*Attila J. Mozer, * Email: attila@uow.edu.au, Tel: +61242981429

REFERENCES

1. Ratcliff, E. L.; Garcia, A.; Paniagua, S. A.; Cowan, S. R.; Giordano, A. J.; Ginley, D. S.; Marder, S. R.; Berry, J. J.; Olson, D. C., Investigating the Influence of Interfacial Contact Properties on Open Circuit Voltages in Organic Photovoltaic Performance: Work Function Versus Selectivity. Advanced Energy Materials 2013, 3 (5), 647-656.

2. Ratcliff, E. L.; Zacher, B.; Armstrong, N. R., Selective Interlayers and Contacts in Organic Photovoltaic Cells. *The Journal of Physical Chemistry Letters* **2011,** *2* (11), 1337-1350.

3. Zacher, B.; Gantz, J. L.; Richards, R. E.; Armstrong, N. R., Organic Solar Cells—At the Interface. *The Journal of Physical Chemistry Letters* **2013,** *4* (11), 1949-1952.

4. Jasieniak, J. J.; Seifter, J.; Jo, J.; Mates, T.; Heeger, A. J., A Solution-Processed MoO_x Anode Interlayer for Use within Organic Photovoltaic Devices. *Advanced Functional Materials* **2012,** *22* (12), 2594-2605.

5. Kim, J. Y.; Kim, S. H.; Lee, H. H.; Lee, K.; Ma, W.; Gong, X.; Heeger, A. J., New Architecture for High-Efficiency Polymer Photovoltaic Cells Using Solution-Based Titanium Oxide as an Optical Spacer. *Advanced Materials* **2006,** *18* (5), 572-576.

6. Gilot, J.; Barbu, I.; Wienk, M. M.; Janssen, R. A. J., The Use of ZnO as Optical Spacer in Polymer Solar Cells: Theoretical and Experimental Study. *Applied Physics Letters* **2007,** *91* (11), 113520-113523.

7.   Bovill, E.; Yi, H.; Iraqi, A.; Lidzey, D. G., The Fabrication of Polyfluorene Stable Process Route. *Applied Physics Letters* **2014,** *105* (22), 223302-223305.

8.   Machui, F.; Hosel, M.; Li, N.; Spyropoulos, G. D.; Ameri, T.; Sondergaard, R. R.; Jorgensen, M.; Scheel, A.; Gaiser, D.; Kreul, K.; Lenssen, D.; Legros, M.; Lemaitre, N.; Vilkman, M.; Valimaki, M.; Nordman, S.; Brabec, C. J.; Krebs, F. C., Cost Analysis of Roll-to-Roll Fabricated ITO Free Single and Tandem Organic Solar Modules Based on Data from Manufacture. *Energy & Environmental Science* **2014,** *7* (9), 2792-2802.

9.   Jørgensen, M.; Norrman, K.; Gevorgyan, S. A.; Tromholt, T.; Andreasen, B.; Krebs, F. C., Stability of Polymer Solar Cells. *Aaterials* **2012,** *24* (5), 580-612.

10.   Min, J.; Luponosov, Y. N.; Zhang, Z.-G.; Ponomarenko, S. A.; Ameri, T.; Li, Y.; Brabec, C. J., Interface Design to Improve the Performance and Stability of Solution-Processed Small-Molecule Conventional Solar Cells. *Advanced Energy Materials* **2014,** *4* (16), 1400816.

11.   Liang, Y.; Xu, Z.; Xia, J.; Tsai, S*dvanced M*
.-T.; Wu, Y.; Li, G.; Ray, C.; Yu, L., For the Bright Future—Bulk Heterojunction Polymer Solar Cells with Power Conversion Efficiency of 7.4%. *Advanced Materials* **2010,** *22* (20), E135-E138.

12.   Zhao, L.; Zhao, S.; Xu, Z.; Yang, Q.; Huang, D.; Xu, X., A Simple Method to Adjust the Morphology of Gradient Three-Dimensional PTB7-Th:PC71BM Polymer Solar Cells. *Nanoscale* **2015,** *7* (12), 5537-5544.

13.   Lu, L.; Yu, L., Understanding Low Bandgap Polymer PTB7 and Optimizing Polymer Solar Cells Based on It. *Advanced Materials* **2014,** *26* (26), 4413-4430.

14.   Wright, B. F.; Sunahara, K.; Furube, A.; Nattestad, A.; Clarke, T. M.; Bazan, G. C.; Azoulay, J. D.; Mozer, A. J., Driving Force Dependence of Electron Transfer Kinetics and Yield

in Low-Band-Gap Polymer Donor–Acceptor Organic Photovoltaic Blends. *The Journal of Physical Chemistry C* **2015,** *119* (23), 12829-12837.

15. Chen, S.; Manders, J. R.; Tsang, S.-W.; So, F., Metal Oxides for Interface Engineering in Polymer Solar Cells. *Journal of Materials Chemistry* **2012,** *22* (46), 2422-24212.

16. Kang, T. E.; Cho, H. H.; Cho, C. H.; Kim, K. H.; Kang, H.; Lee, M.; Lee, S.; Kim, B.; Im, C.; Kim, B. J., Photoinduced Charge Transfer in Donor-Acceptor (DA) Copolymer: Fullerene Bis-Adduct Polymer Solar Cells. *ACS Appl Mater Interfaces* **2013,** *5* (3), 861-868.

17. Li, H.; Earmme, T.; Subramaniyan, S.; Jenekhe, S. A., Bis(Naphthalene Imide)diphenylanthrazolines: A New Class of Electron Acceptors for Efficient Nonfullerene Organic Solar Cells and Applicable to Multiple Donor Polymers. *Advanced Energy Materials* **2015,** *5* (8), 1402041.

18. Greiner, M. T.; Lu, Z.-H., Thin-Film Metal Oxides in Organic Semiconductor Devices: Their Electronic Structures, Work Functions and Interfaces. *NPG Asia Mater* **2013,** *5* (7), e55.

19. You, J.; Dou, L.; Yoshimura, K.; Kato, T.; Ohya, K.; Moriarty, T.; Emery, K.; Chen, C.-C.; Gao, J.; Li, G.; Yang, Y., A Polymer Tandem Solar Cell with 10.6% Power Conversion Efficiency. *Nat Commun* **2013,** *4*, 1446.

20. Li, P.; Cai, L.; Wang, G.; Zhou, D. C.; Xiang, J.; Zhang, Y. J.; Ding, B. F.; Alameh, K.; Song, Q. L., PEIE Capped ZnO as Cathode Buffer Layer with Enhanced Charge Transfer Ability for High Efficiency Polymer Solar Cells. *Synth. Met.* **2015,** *203*, 243-248.

21. Bovill, E.; Scarratt, N.; Griffin, J.; Yi, H.; Iraqi, A.; Buckley, A. R.; Kingsley, J. W.; Lidzey, D. G., The Role of the Hole-Extraction Layer in Determining the Operational Stability of a Polycarbazole:Fullerene Bulk-Heterojunction Photovoltaic Device. *Applied Physics Letters* **2015,** *106* (7), 073301-073305.

22.   Shrotriya, V.; Li, G.; Yao, Y.; Chu, C.-W.; Yang, Y., Transition Metal Oxides as the Buffer layer for Polymer Photovoltaic Cells. *Applied Physics Letters* **2006,** *88* (7), 073508.

23.   Kim, D. Y.; Subbiah, J.; Sarasqueta, G.; So, F.; Ding, H.; Irfan; Gao, Y., The Effect of Molybdenum Oxide Interlayer on Organic Photovoltaic Cells. *Applied Physics Letters* **2009,** *95* (9), 093304.

24.   Meyer, J.; Khalandovsky, R.; Gorrn, P.; Kahn, A., MoO$_3$ Films Spin-Coated from a Nanoparticle Suspension for Efficient Hole-Injection in Organic Electronics. *Advanced materials* **2011,** *23* (1), 70-73.

25.   Bovill, E. S. R.; Griffin, J.; Wang, T.; Kingsley, J. W.; Yi, H.; Iraqi, A.; Buckley, A. R.; Lidzey, D. G., Air Processed Organic Photovoltaic Devices Incorporating a MoO$_x$ Anode Buffer Layer. *Applied Physics Letters* **2013,** *102* (18), 183303.

26.   Liu, J.; Wu, X.; Chen, S.; Shi, X.; Wang, J.; Huang, S.; Guo, X.; He, G., Low-Temperature MoO$_3$ Film from a Facile Synthetic Route for an Efficient Anode Interfacial Layer in Organic Optoelectronic Devices. *Journal of Materials Chemistry C* **2014,** *2* (1), 158-163.

27.   Sun, Y.; Takacs, C. J.; Cowan, S. R.; Seo, J. H.; Gong, X.; Roy, A.; Heeger, A. J., Efficient, Air-Stable Bulk Heterojunction Polymer Solar Cells Using MoO$_x$ as the Anode Interfacial Layer. *Advanced Materials* **2011,** *23* (19), 2226-2230.

28.   Murase, S.; Yang, Y., Solution Processed MoO$_3$ Interfacial Layer for Organic Photovoltaics Prepared by a Facile Synthesis Method. *Advanced Materials* **2012,** *24* (18), 2459-2462.

29.   Yi, Q.; Zhai, P.; Sun, Y.; Lou, Y.; Zhao, J.; Sun, B.; Patterson, B.; Luo, H.; Zhang, W.; Jiao, L.; Wang, H.; Zou, G., Aqueous Solution-Deposited Molybdenum Oxide Films as an Anode Interfacial Layer for Organic Solar Cells. *ACS Appl Mater Interfaces* **2015,** *7* (33), 18218-18224.

30.   Widjonarko, N. E.; Schulz, P.; Parilla, P. A.; Perkins, C. L.; Ndione, P. F.; Sigdel, A. K.; Olson, D. C.; Ginley, D. S.; Kahn, A.; Toney, M. F.; Berry, J. J., Impact of Hole Transport Layer Surface Properties on the Morphology of a Polymer-Fullerene Bulk Heterojunction. *Advanced Energy Materials* **2014,** *4* (11), 1301879.

31.   Ko, C.; Yang, Z.; Ramanathan, S., Work Function of Vanadium Dioxide Thin Films Across the Metal-Insulator Transition and the Role of Surface Nonstoichiometry. *ACS Appl Mater Interfaces* **2011,** *3* (9), 3396-3401.

32.   Tao, C.; Ruan, S.; Xie, G.; Kong, X.; Shen, L.; Meng, F.; Liu, C.; Zhang, X.; Dong, W.; Chen, W., Role of Tungsten Oxide in Inverted Polymer Solar Cells. *Applied Physics Letters* **2009,** *94* (4), 043311.

33.   Kim, J. Y.; Lee, K.; Coates, N. E.; Moses, D.; Nguyen, T.-Q.; Dante, M.; Heeger, A. J., Efficient Tandem Polymer Solar Cells Fabricated by All-Solution Processing. *Science* **2007,** *317* (5835), 222-225.

34.   Yang, D.; Fu, P.; Zhang, F.; Wang, N.; Zhang, J.; Li, C., High Efficiency Inverted Polymer Solar Cells with Room-Temperature Titanium Oxide/Polyethylenimine Films as Electron transport Layers. *J Mater Chem A* **2014,** *2* (41), 17281-17285.

35.   Park, S. H.; Roy, A.; Beaupré, S.; Cho, S.; Coates, N.; Moon, J. S.; Moses, D.; Leclerc, M.; Lee, K.; Heeger, A. J., Bulk Heterojunction Solar Cells with Internal Quantum Efficiency Approaching 100%. *Nature Photonics* **2009,** *3* (5), 297-302.

36.   Lin, Z.; Chang, J.; Zhang, J.; Jiang, C.; Wu, J.; Zhu, C., A Work-Function Tunable Polyelectrolyte Complex (PEI:PSS) as a Cathode Interfacial Layer for Inverted Organic Solar Cells. *J Mater Chem A* **2014,** *2* (21), 7788-7794.

37.   Yan, L.; Song, Y.; Zhou, Y.; Song, B.; Li, Y., Effect of PEI Cathode Interlayer on Work Function and Interface Resistance of ITO Electrode in the Inverted Polymer Solar Cells. *Organic Electronics* **2015,** *17* (0), 94-101.

38.   Zhou, Y.; Fuentes-Hernandez, C.; Shim, J.; Meyer, J.; Giordano, A. J.; Li, H.; Winget, P.; Papadopoulos, T.; Cheun, H.; Kim, J.; Fenoll, M.; Dindar, A.; Haske, W.; Najafabadi, E.; Khan, T. M.; Sojoudi, H.; Barlow, S.; Graham, S.; Brédas, J.-L.; Marder, S. R.; Kahn, A.; Kippelen, B., A Universal Method to Produce Low–Work Function Electrodes for Organic Electronics. *Science* **2012,** *336* (6079), 327-332.

39.   Choi, H.; Kim, H. B.; Ko, S. J.; Kim, J. Y.; Heeger, A. J., An Organic Surface Modifier to Produce a High Work Function Transparent Electrode for High Performance Polymer Solar Cells. *Advanced Materials* **2015,** *27* (5), 892-896.

40.   Kirchartz, T.; Deledalle, F.; Tuladhar, P. S.; Durrant, J. R.; Nelson, J., On the Differences between Dark and Light Ideality Factor in Polymer:Fullerene Solar Cells. *The Journal of Physical Chemistry Letters* **2013,** *4* (14), 2371-2376.

41.   Reinhardt, J.; Grein, M.; Bühler, C.; Schubert, M.; Würfel, U., Identifying the Impact of Surface Recombination at Electrodes in Organic Solar Cells by Means of Electroluminescence and Modeling. *Advanced Energy Materials* **2014**, *4* (11), 1400081.

42.   Wheeler, S.; Deledalle, F.; Tokmoldin, N.; Kirchartz, T.; Nelson, J.; Durrant, J. R., Influence of Surface Recombination on Charge-Carrier Kinetics in Organic Bulk Heterojunction Solar Cells with Nickel Oxide Interlayers. *Physical Review Applied* **2015,** *4* (2), 024020.

43.   Elliott, L. C. C.; Basham, J. I.; Pernstich, K. P.; Shrestha, P. R.; Richter, L. J.; DeLongchamp, D. M.; Gundlach, D. J., Probing Charge Recombination Dynamics in Organic

Photovoltaic Devices under Open-Circuit Conditions. *Advanced Energy Materials* **2014,** *4* (15), 1400356.

44.   Spies, A.; List, M.; Sarkar, T.; Würfel, U., On the Impact of Contact Selectivity and Charge Transport on the Open-Circuit Voltage of Organic Solar Cells. *Advanced Energy Materials* **2017,** *7* (5), 1601750.

45.   Barnes, P. R.; Miettunen, K.; Li, X.; Anderson, A. Y.; Bessho, T.; Gratzel, M.; O'Regan, B. C., Interpretation of Optoelectronic Transient and Charge Extraction Measurements in Dye-Sensitized Solar Cells. *Advanced Materials* **2013,** *25* (13), 1881-1922.

46.   Katoh, R.; Kasuya, M.; Kodate, S.; Furube, A.; Fuke, N.; Koide, N., Effects of 4-tert-Butylpyridine and Li Ions on Photoinduced Electron Injection Efficiency in Black-Dye-Sensitized Nanocrystalline TiO2 Films. *The Journal of Physical Chemistry C* **2009,** *113* (48), 20738-20744.

47.   Cravino, A.; Schilinsky, P.; Brabec, C. J., Characterization of Organic Solar Cells: the Importance of Device Layout. *Advanced Functional Materials* **2007,** *17* (18), 3906-3910.

48.   Valle, B.; Loser, S.; Hennek, J. W.; DeGeorge, V.; Klosterman, C.; Andrews, J. H.; Singer, K. D.; Marks, T. J., Spectral Aspects of Cavity Tuned Absorption in Organic Photovoltaic Films. *Optics express* **2012,** *20 Suppl 6*, A954-A963.

49.   Wright, B.; Nakajima, Y.; Clarke, T. M.; Okuda, K.; Paananen, H.; Mozer, A. J.; Mori, S., Quantifying Recombination Losses during Charge Extraction in Bulk Heterojunction Solar Cells Using a Modified Charge Extraction Technique. *Advanced Energy Materials* **2017,** *7* (11), 1602026.

50. Clarke, T. M.; Lungenschmied, C.; Peet, J.; Drolet, N.; Mozer, A. J., A Comparison of Five Experimental Techniques to Measure Charge Carrier Lifetime in Polymer / Fullerene Solar Cells. *Advanced Energy Materials*, **2015**, *5*, 1401345.

51.   Kuwabara, T.; Sugiyama, H.; Yamaguchi, T.; Takahashi, K., Inverted type Bulk-Heterojunction Organic Solar Cell Using Electrodeposited Titanium Oxide Thin Films as Electron Collector Electrode. *Thin Solid Films* **2009,** *517* (13), 3766-3769.

52.   Deledalle, F.; Shakya Tuladhar, P.; Nelson, J.; Durrant, J. R.; Kirchartz, T., Understanding the Apparent Charge Density Dependence of Mobility and Lifetime in Organic Bulk Heterojunction Solar Cells. *The Journal of Physical Chemistry C* **2014,** *118* (17), 8837-8842.

53.   Shi, H.; Liu, C.; Jiang, Q.; Xu, J., Effective Approaches to Improve the Electrical Conductivity of PEDOT:PSS: A Review. *Advanced Electronic Materials* **2015,** *1* (4), 1500017.

54.   Lenze, M. R.; Kronenberg, N. M.; Würthner, F.; Meerholz, K., In-situ Modification of PEDOT:PSS Work Function Using Alkyl Alcohols as Secondary Processing Solvents and Their Impact on Merocyanine Based Bulk Heterojunction Solar Cells. *Organic Electronics* **2015,** *21*, 171-176.

55.   Guan, Z.; Li, H.-W.; Cheng, Y.; Yang, Q.; Lo, M.-F.; Ng, T.-W.; Tsang, S.-W.; Lee, C.-S., Charge-Transfer State Energy and Its Relationship with Open-Circuit Voltage in an Organic Photovoltaic Device. *The Journal of Physical Chemistry C* **2016,** *120* (26), 14059-14068.

56.   Tang, Z.; Wang, J.; Melianas, A.; Wu, Y.; Kroon, R.; Li, W.; Ma, W.; Andersson, M. R.; Ma, Z.; Cai, W.; Tress, W.; Inganäs, O., Relating Open-Circuit Voltage Losses to the Active Layer Morphology and Contact Selectivity in Organic Solar Cells. *J Mater Chem A* **2018,** *6* (26), 12574-12581.

57.   Andersen, T. R.; Almyahi, F.; Cooling, N. A.; Elkington, D.; Wiggins, L.; Fahy, A.; Feron, K.; Vaughan, B.; Griffith, M. J.; Mozer, A. J.; Sae-kung, C.; Wallace, G. G.; Belcher, W. J.; Dastoor, P. C., Comparison of Inorganic Electron Transport Layers in Fully Roll-to-Roll Coated/Printed Organic Photovoltaics in Normal Geometry. *J Mater Chem A* **2016,** *4* (41), 15986-15996.

58.   Clarke, T. M.; Lungenschmied, C.; Peet, J.; Drolet, N.; Sunahara, K.; Furube, A.; Mozer, A. J., Photodegradation in Encapsulated Silole-Based Polymer: PCBM Solar Cells Investigated Using Transient Absorption Spectroscopy and Charge Extraction Measurements. *Advanced Energy Materials* **2013,** *3* (11), 1473-1483.

59.   Clarke, T. M.; Peet, J.; Denk, P.; Dennler, G.; Lungenschmied, C.; Mozer, A. J., Non-Langevin Bimolecular Recombination in a Silole-based Polymer:PCBM Solar Cell Measured by Time-Resolved Charge Extraction and Resistance-Dependent Time-of-Flight Techniques. *Energy & Environmental Science* **2012,** *5* (1), 5241-5245.

Table of Contents Image